Absolute linear-in-k spectrometer designs enabled by freeform optics

CHANGSIK YOON, 1,* D AARON BAUER, 1 DI XU, 1 D CHRISTOPHE DORRER, 2 D AND JANNICK P. ROLLAND1

 1 The Institute of Optics, University of Rochester, 275 Hutchison Road, Rochester, NY 14627, USA ²Laboratory for Laser Energetics, University of Rochester, 250 East Road, Rochester, NY 14623, USA *cyoon6@ur.rochester.edu

Abstract: Linear-in-wavenumber, k, spectrometers have the merits of saving signal processing time and improving the sensitivity of spectral-domain optical coherence tomography (SD-OCT) by avoiding post-k-interpolation. We report on an approach leveraging freeform optics to linearize spectrometers in k to achieve an extremely low residual k-nonlinearity in design. A freeform lens reduced the k-nonlinearity from 2.47% for a benchmark spectrometer to 2.79×10^{-5} % and 3.36 \times 10⁻⁹% using the Fringe Zernike coefficients up to the 16th term and 37th term, respectively. A simulation model was developed to evaluate the performance of SD-OCT with the designed spectrometers. Without the k-interpolation in software, results show that the two freeform spectrometers achieve a roll-off gain of 5.24 dB over the imaging depth from 0.5 to 5.5 mm, while the maximum imaging depth is 5.8 mm. Finally, a 4.2-µm-FWHM axial PSF was maintained throughout the imaging depth in air.

© 2019 Optical Society of America under the terms of the OSA Open Access Publishing Agreement

1. Introduction

A conventional spectrometer has intrinsic nonlinearity in wavenumber, k, over the camera pixels due to the nonlinear angular dispersion in k corresponding to its inherent dispersion element, i.e., a grating or prism. For spectrometers used in spectral-domain optical coherence tomography (SD-OCT), this nonlinearity requires post-processing, i.e., linear k-interpolation, before the fast Fourier transform (FFT). Various options to mitigate the non-linearity issue in software with corresponding trade-offs are covered in a prior art [1]. This post-processing not only slows the total imaging speed but, more importantly, adds a numerical error into each SD-OCT A-scan by the inaccuracy of the numerical interpolation, the level of which is approximately proportional to the square of imaging depth [2].

In 1990, the nonlinear angular dispersion for k was first linearized using a grism [3]. This idea evolved into using a custom prism that is separated from a grating, providing more degrees of freedom to linearize the angular dispersion [4,5]. The spectrometer was further optimized using parameters of the prism material, rotation angle between the grating and the prism [6], groove density of the grating [7], and prism vertex angle [8]. More recently, a ray-trace model of a linear-in-k spectrometer was reported using a BK7 prism with an optimized vertex angle [9]. In the prior arts, the linear-in-k spectrometer reduced the k-nonlinearity over the camera pixels, and it showed a peak roll-off gain in the experimental comparison with the conventional spectrometer using the post-k-interpolation.

Given that it is well established experimentally that the spectral resolution, the nonlinearity relative to wavenumber, and the accuracy in the spectrometer calibration all affect the roll-off and the axial resolution [2,10], in this paper, we resort to simulations in order to isolate these factors. Specifically, the simulations enable eliminating the impact of the spectrometer calibration. Also, by design, we maintain a constant spectral resolution. This approach allows us to investigate the isolated impact of the linear-in-k property on the roll-off and the axial resolution quantified as the full width at half maximum (FWHM) of the OCT axial point spread function (PSF). Besides,

#375225 Journal © 2019

it is essential to establish how close to 100% *k*-linearity we must reach to not only reduce the roll-off but also maintain the axial resolution throughout the imaging depth.

In this paper, we report on an *absolute*-linear-in-*k* spectrometer, designed based on a *benchmark* spectrometer, while preserving the spectral resolution provided by the *benchmark*. The novel approach to the *k*-linearization uses the emerging technology of freeform optics. We show that the use of freeform optics remarkably reduces the residual nonlinearity (RN) to the point where any further reduction in RN has no significant improvement on both the peak roll-off and FWHMs of the axial PSFs throughout the imaging depth.

2. Design process of freeform spectrometers

A freeform optics has a surface geometry that has translational and rotational variance about the optics axis. The advantages of freeform optics have been shown for optimal aberration correction in either an electronic viewfinder [11] or a three-mirror imager [12] and for compactness in a mirror-type spectrometer [13].

The design process of the freeform linear-in-*k* spectrometer is presented as follows. First, a lens-type *benchmark* spectrometer was prepared using commercial optical design software, CODEV, as shown in Fig. 1(a). The *benchmark* spectrometer operates in the near-infrared (NIR), i.e., 790-900 nm, and has spectral resolution ranging from 0.035 nm to 0.052 nm. Second, a CaF₂-Brewster angled prism (BAP) was inserted right after the grating of the *benchmark*, which we named *quasi*-linear-in-*k* spectrometer. We define *quasi*-k-linearity as a hardware-based *k*-linearity with which a spectrometer shows a broadening of the axial PSFs over the imaging depth when a Fourier transformation is performed on the measured spectra without a software linear interpolation method. When this broadening is not present, we define the linearity as *absolute-k*-linearity. The evaluation of axial PSFs over the imaging depth will be presented in Section 4. Then, the overall alignment was optimized to minimize the *k*-nonlinearity, using variables of the rotation angle of the grating, rotation angle of the prism, air-thickness between the grating and the prism, and distance between the prism and the objective lens. Finally, the rear surface of the field lens was modified to adopt a freeform shape, as shown in Fig. 1(b), where the freeform sag was mathematically described using Fringe Zernike polynomials [14] given as

$$z = \frac{cr^2}{1 + \sqrt{1 - (1 + k_c)c^2r^2}} + \sum_j C_j Z_j(\rho, \varphi), \tag{1}$$

where z is the sag of the surface, r is the radial coordinate of the surface, c is the curvature of the base sphere, k_c is the conic constant, ρ and φ are the normalized radial and azimuthal components in the aperture, and C_i is the weight factor of the jth Fringe Zernike term, Z_i . The freeform surface was designed with a custom merit function. The function was constructed to minimize the root-mean-square (RMS) spot sizes of design wavelengths evenly spaced in k while constraining the chief ray heights of the design wavelengths to be evenly separated at the detector plane. During the optimization, piston and defocus by the freeform surface were constrained while varying the following design parameters: The coefficients C_i with symmetry about the Y-axis [see the axis in Fig. 1(b)], conic constant k_c , air-thickness between the field lens and the detector, and tilt of the detector plane about the X-axis. Two spectrometer designs were created to investigate the impact of the RN on the OCT imaging performance: Design#1 was made using sixteen Fringe Zernike terms, Z_1 to Z_{16} , and Design#2 extended to thirty-seven terms, Z_1 to Z_{37} . Both freeform field lenses are made of Schott NBK-7 glass that may be ground and polished to their freeform shapes. For best visualizing the freeform sags, as illustrated in Fig. 1(c), the effective rectangular aperture, 41 mm × 5 mm, of the two freeform surfaces of Design#1 and #2 underwent the rigid body rotation and piston-removal to have zero mean tilt. Then, the base spherical components were removed within the effective aperture.

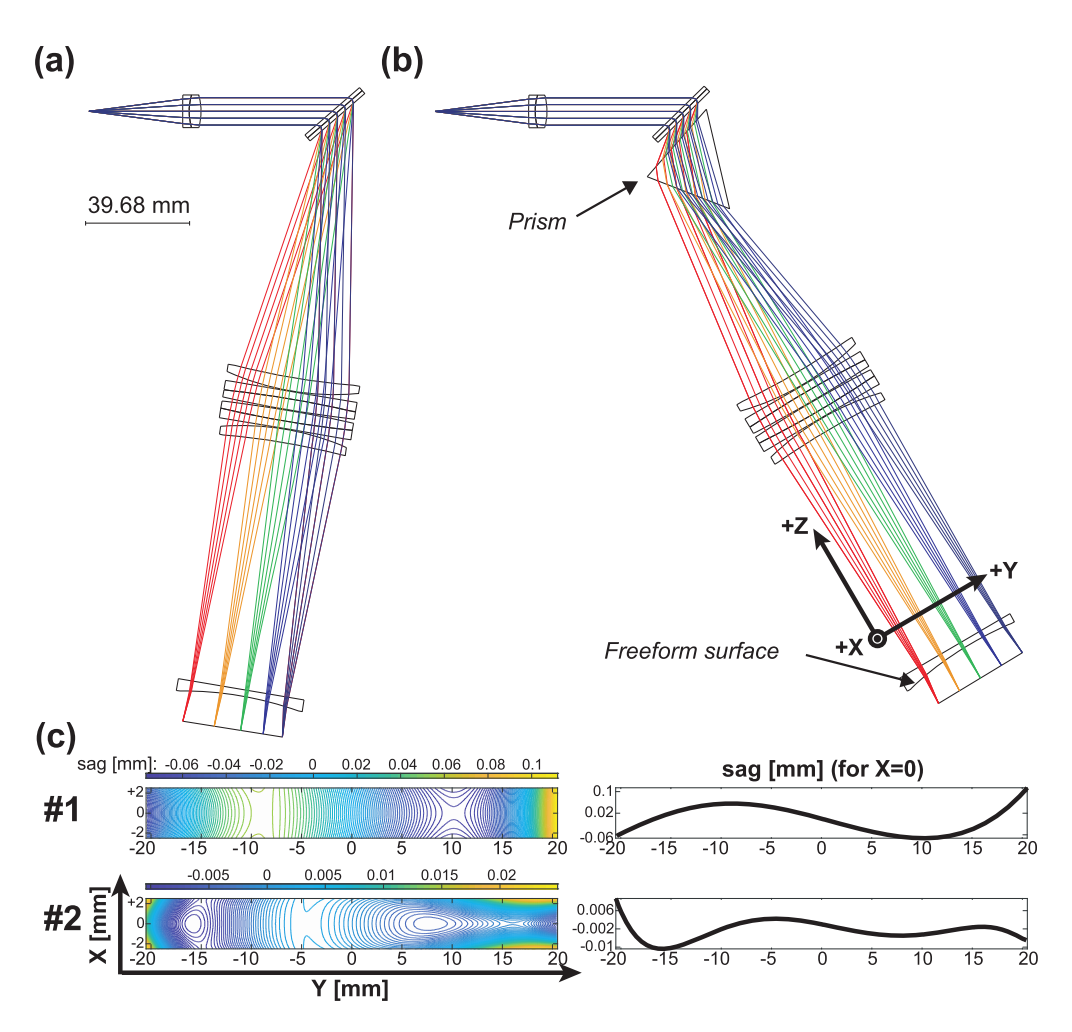


Fig. 1. Optical layout of (a) the *benchmark* spectrometer and (b) the *absolute*-linear-in-k spectrometer with the CaF₂-BAP and the freeform field lens. (c) Freeform sags of the field lenses of Design#1 and #2 within the effective rectangular aperture, 41 mm \times 5 mm.

3. Residual k-nonlinearity and spectral resolution

The RN of each spectrometer was quantified using a unitless nonlinearity metric [15] defined as

$$RN[\%] = \frac{\sqrt{\left(\int_{k_{\min}}^{k_{\max}} \left[f(k) - g(k)\right]^2 dk\right) / (k_{\max} - k_{\min})}}{f(k_{\max}) - f(k_{\min})} \times 100,$$
(2)

where $k_{\rm max}$ and $k_{\rm min}$ are the maximum and minimum wavenumbers, respectively, f(k) is the calibration function relating wavenumber to camera pixel, and g(k) is the linear fit of f(k) with the least RMS error. The RN of the *benchmark* spectrometer was 2.47%, which dropped to 0.05% after adding the CaF2-BAP in the *quasi*-linear-in-k spectrometer. By using the freeform surface, the RN was further decreased to $2.79 \times 10^{-5}\%$ for Design#1 and $3.36 \times 10^{-9}\%$ for Design#2, as shown in Fig. 2(a). Figure 2(b) shows f(k) - g(k) after ensuring that f(k) - g(k) equals zero for the central k across the four spectrometers. The optimization with the higher order terms, up to $37^{\rm th}$, allowed for more local control over the freeform surface compared to the optimization with

only the lower order terms, up to 16^{th} . This local control enabled the linearization of the ks more readily together with less departure of the freeform surface from a sphere. The lower-order terms did not have as much degrees of freedom and thus needed more departure to accomplish the task. Therefore, the overall sags of Design#1 and #2 are differentiated.

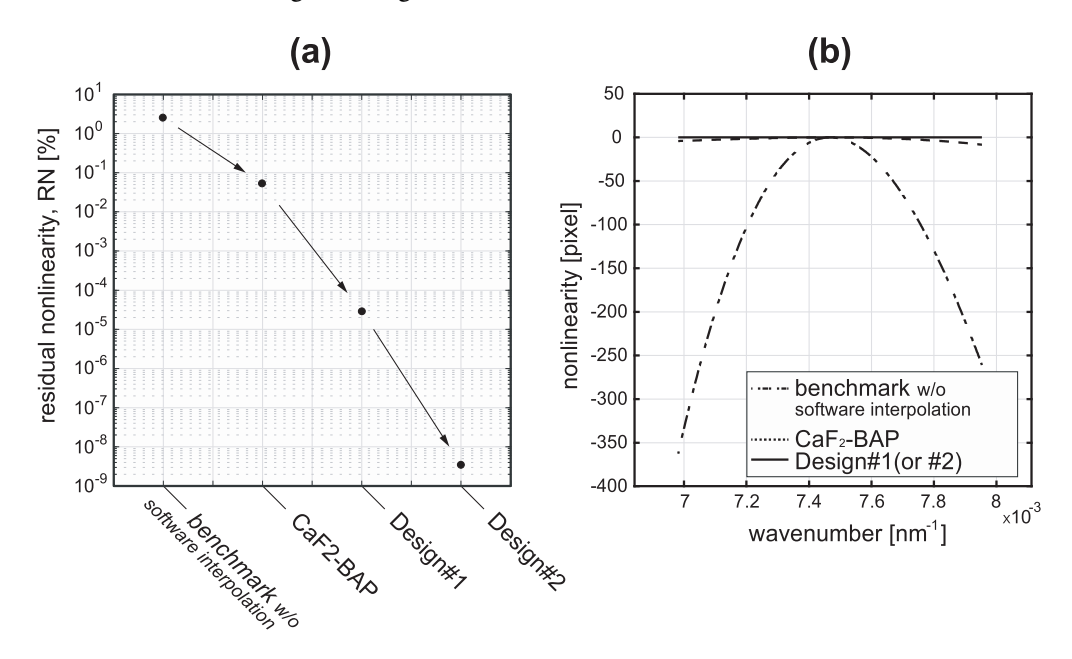


Fig. 2. Metrics of *k*-nonlinearity: (a) logarithmic RNs for the four spectrometers, showing dramatic decrease after implementing the freeform field lenses and (b) pixel errors by the RNs of the *benchmark*, CaF2-BAP, and freeform spectrometers when the total number of camera pixels is 4096.

We defined the spectral resolution as the spectral bandwidth effectively measured by one pixel [16]. The spectral resolution was computed based on a line-scan camera of 4096 pixels with

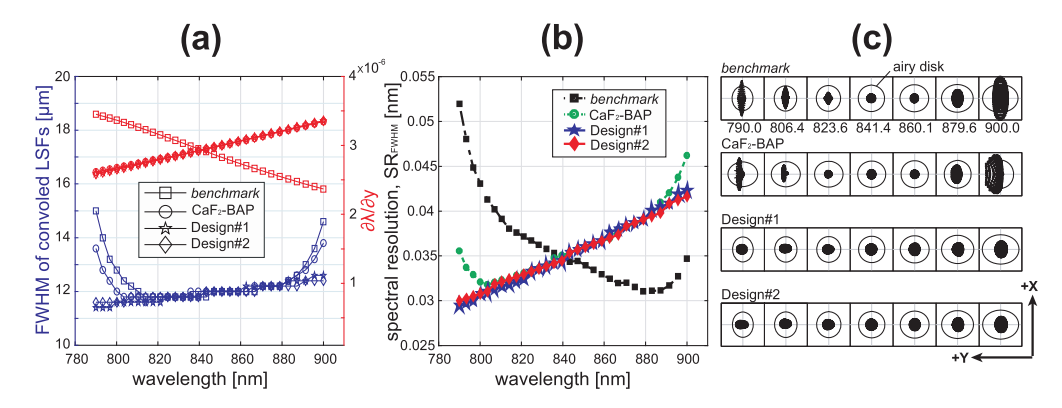


Fig. 3. Performance metrics for the *benchmark*, CaF_2 -BAP, and two freeform spectrometers: (a) FWHMs of LSFs convolved with a 10- μ m-window (left axis, in blue) and derivatives of wavelengths (right axis, in red), (b) spectral resolution, and (c) spot diagrams. Note that the derivatives of wavelengths for the CaF_2 -BAP and two freeform spectrometers are near equivalent, as shown by the overlapping symbols.

a 10-µm-width pixel. Each pixel was modeled as a 10-µm-width rectangular window, and the window was convolved with line spread functions (LSFs) of evenly-spaced ks for estimating the effective spectrum collected by one pixel. Then, the FWHM of the convolved LSFs, as shown in Fig. 3(a), was converted to the spectral FWHM by multiplying the FWHM with derivatives of the wavelengths over the detector plane along the y-axis, $\partial \lambda/\partial y$, as shown in Fig. 3(b). The spectral resolutions are illustrated in Fig. 3(b) for the four spectrometers, i.e., the benchmark, CaF₂-BAP, and two freeform spectrometers. The average spectral resolution taken with thirty evenly-spaced ks remained the same as 0.036 nm even after adding the CaF₂-BAP, but the spectral resolution increased as the wavelength increased (or, as the wavenumber decreased). The relationship indeed manifests the k-linearity as the spectral resolution is mainly determined by the width of the lateral PSF, proportional to the wavelength. However, adding the prism into the benchmark spectrometer introduced a field-dependent coma, as observed in the spot diagram of the quasi-linear-in-k spectrometer with the CaF₂-BAP in Fig. 3(c), which did not exist in the benchmark spectrometer. The field-dependent coma is caused by a k-dependent stop shift due to the prism. Figure 4 illustrates the chief rays traced in an example setup from a grating point, G, to a lens. By the prism, the lens sees the maximum and minimum ks departing at z_1 and z_2 , respectively, with an axial spread of the stop position Δ .

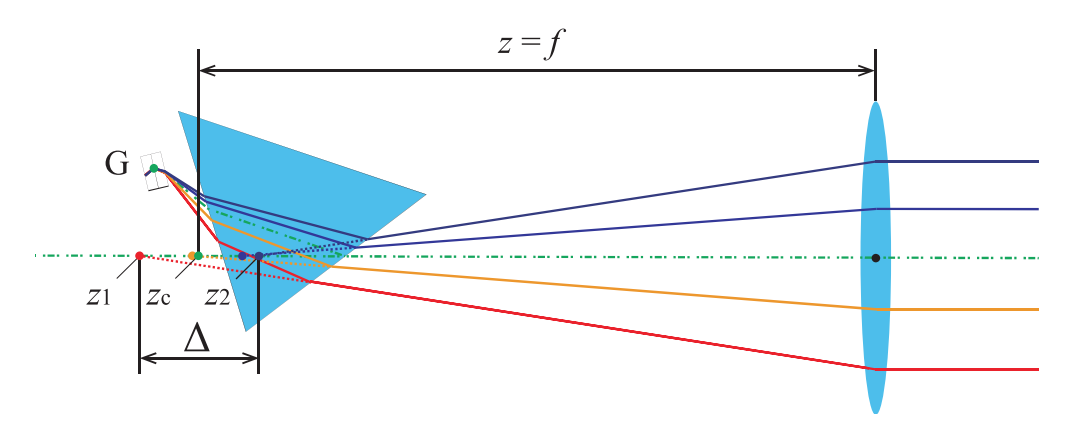


Fig. 4. The *k*-dependent stop shifts by the prism cause the field-dependent coma in the CaF₂-BAP spectrometer.

4. Simulation-based imaging performance

In theory, the FWHM of axial PSF in SD-OCT is given by the central wavelength and bandwidth of a light source [17]. However, in practice, both the calibration accuracy of a spectrometer and dispersion mismatch between the reference and sample beams significantly affect the actual FWHM of the axial PSF in the experiment. To rule out those factors in the evaluation of imaging performance, we simulated the axial PSFs for the different spectrometer designs.

According to the Wiener-Khinchin theorem, the coherence function, $\Gamma(\tau)$, is the inverse FT of a spectral density of a source, $S(\nu)$. In SD-OCT, the spectral resolution of a spectrometer impacts the fringe visibility of the measured modulation, and the axial PSF rolls off with increasing time delay τ between the reference and sample beams [17]. The roll-off has been well understood with both a Gaussian source and uniform spectral resolutions over ks. Here, we develop a mathematical expression named the localized coherence function to handle various source shapes and non-uniform spectral resolutions. The localized spectral density is the spectral density collected by the ith camera pixel and can be obtained by convolving k-dependent lateral PSFs with the ith pixel window. The localized spectral density, denoted as iS(ν), can be approximately

expressed with a normalized Gaussian function of the optical frequency, ν , weighted by alpha, α , that accounts for the shape of the source, which is given as

$${}^{i}S(\nu) = \frac{{}^{i}\alpha}{\sqrt{2\pi} \cdot {}^{i}\delta_{\nu}} \exp\left[\frac{-(\nu - {}^{i}\nu)^{2}}{2{}^{i}\delta_{\nu}^{2}}\right],\tag{3}$$

assuming the total spectral density is conserved as

$$\sum_{i=1}^{N} {}^{i}S(\nu) \cong S(\nu), \tag{4}$$

where ${}^{i}v$ is the mean optical frequency focused on the i^{th} pixel, ${}^{i}\delta_{v}$ is the standard deviation of ${}^{i}S(v)$, and N is the total number of the camera pixels. For simplicity, we assumed uniformity in the diffraction efficiency over the optical frequency as well as no additional attenuation by the prism and the lenses.

The standard deviation of the localized spectral density, ${}^{i}\delta_{\nu}$, is related to the FWHM spectral resolution, SR_{FWHM} , which can be obtained from the optical designs of the four spectrometers [See Fig. 3(b)], by a constant factor as

$${}^{i}\delta_{\nu} = \frac{1}{2\sqrt{2\ln 2}} \cdot {}^{i}SR_{FWHM}. \tag{5}$$

Taking the inverse FT of ${}^{i}S(\nu)$ in Eq. (3), the localized coherence function can be obtained as

$${}^{i}\Gamma(\tau) = {}^{i}\alpha \cdot \exp\left[\frac{-\tau^2}{1/(2^{i}\delta_{\nu}^2\pi^2)}\right] \cdot \exp[-j2\pi^{i}\nu\tau]. \tag{6}$$

For a spectrometer used in SD-OCT, pixel *i* records the intensity of the interference, ${}^{i}I$, which is the auto-correlation of the total field, ${}^{i}E_{D}$, averaged over exposure time, T, as

$${}^{i}I = \frac{{}^{i}\rho}{2} \left\langle {}^{i}E_{D}^{*}(t){}^{i}E_{D}(t) \right\rangle_{T},\tag{7}$$

where

$${}^{i}E_{D}(t) = {}^{i}K_{R}{}^{i}E_{0}(t) + \sum_{n} {}^{i}K_{n}{}^{i}E_{0}(t + \tau_{n}), \tag{8}$$

 ${}^{i}E_{0}$ is the analytic representation of the source field arriving at the i^{th} pixel, ${}^{i}K_{R}$ and ${}^{i}K_{n}$ are the reflection coefficients of the reference and n^{th} sample, respectively, and ${}^{i}\rho$ is the quantum efficiency of the i^{th} pixel. Equation (8) is substituted into Eq. (7) to obtain the intensity expressed with the localized coherence function, ${}^{i}\Gamma(\tau)$, in Eq. (6) as

$${}^{i}I = \frac{{}^{i}\rho}{2} \left[\begin{array}{c} \left({}^{i}K_{R} {}^{2} + \sum\limits_{n} {}^{i}K_{n} {}^{2} \right) \cdot {}^{i}\Gamma(0) \\ + 2\text{Re} \left\{ \sum\limits_{n} {}^{i}K_{R} {}^{*i}K_{n} {}^{i}\Gamma(\tau_{n}) + \sum\limits_{l \neq m} {}^{i}K_{l} {}^{*i}K_{m} {}^{i}\Gamma(\tau_{l} - \tau_{m}) \right\} \end{array} \right], \tag{9}$$

with

$${}^{i}\Gamma(\tau) = \left\langle {}^{i}E_{D}^{*}(t){}^{i}E_{D}(t+\tau)\right\rangle_{T}.\tag{10}$$

When ${}^{i}K_{R}$ =1 (a mirror) and ${}^{i}K_{n=1}$ =1 (a mirror) for all i, the intensity data were created using Eq. (9) for the *benchmark*, CaF₂-BAP, and two freeform spectrometers with N = 4096 pixels. The frequency dependence of the detector's quantum efficiency was neglected. Figure 5 illustrates

the spectral density of the source (M-D-840HP, Superlum), the weight α , and the intensity iI as a function of pixel i for three imaging depths: 1, 3, and 5 mm. The weight α in Fig. 5(b) showed an inverse correlation with the spectral resolution in Fig. 3(b). This relationship implies that the spectral resolution does distort the detected spectral density in part. From Eq. (6), the localized coherence function exponentially decays as a function of τ^2 with the effect of the spectral resolution in $^i\delta_v$, which results in a non-uniform loss of the fringe visibility, as shown in Fig. 5(c).

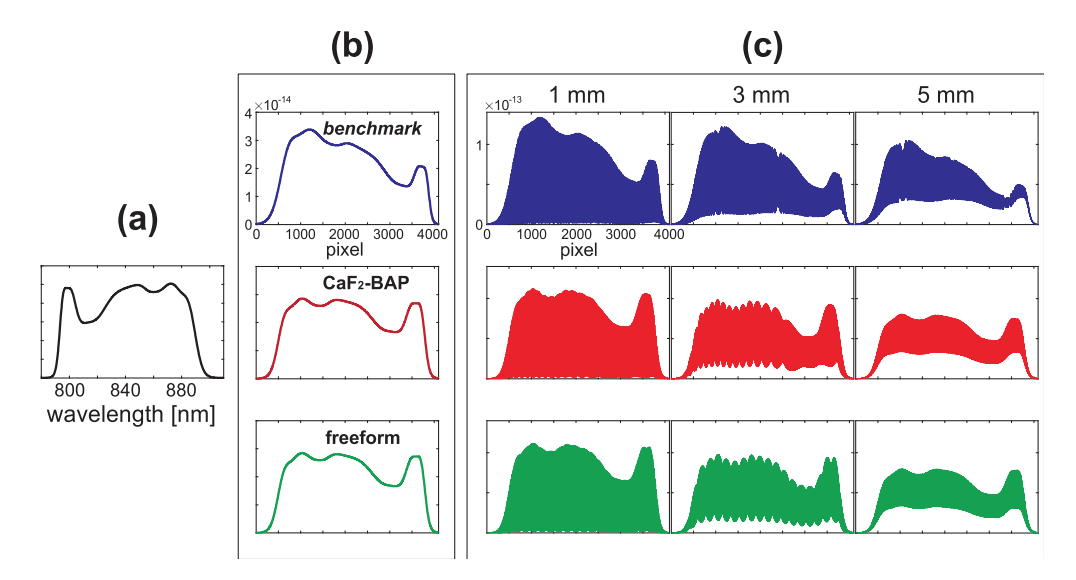


Fig. 5. Simulation of as-measured raw data by the *benchmark* (blue), CaF_2 -BAP (red), freeform-Design#2-spectrometers (green): (a) the spectral density of the source (M-D-840HP, Superlum), (b) the weight α , and (c) the spectral intensity of the interference with optical delays of 1, 3, and 5 mm in the air.

The axial PSFs with various imaging depths of 0.5, 1.5, 2.5, 3.5, 4.5, and 5.5 mm were obtained by directly taking the FFT of the simulated spectra for the CaF₂-BAP and the freeform spectrometers without any spectrum resampling. For the *benchmark* spectrometer, the corresponding spectra were first interpolated along linearly-spaced ks before the FFT. Figure 6 shows the axial PSFs with varying depths. For the *benchmark* spectrometer, the noise-like background is clearly visible, as shown in Fig. 6(a), which is introduced by the k-interpolation error. Also, the floor rises with increasing depth [2]. Such background error was not found in the CaF₂-BAP and the two freeform spectrometers, as shown in Figs. 6(b) and 6(c).

The axial resolution and the roll-off were then evaluated by the FWHM and peak signal power [dB], i.e., $20 \times \text{Log}_{10}[\text{abs}\{\text{FT}\}]$, of the axial PSFs, respectively, at the six evenly spaced imaging depths from 0.5 to 0.5 mm. The *benchmark* spectrometer with the post-*k*-interpolation showed slowly degrading FWHMs ranging from 4.3 to 6.6 µm [see Fig. 7(a)], yet a roll-off of 14.3 dB [see Fig. 7(b)]. In comparison, the CaF₂-BAP spectrometer displayed axial PSFs that were significantly broadened from 4.8 to 29 µm and a roll-off of 16.7 dB. The two freeform spectrometers commonly showed invariant 4.2-µm-FWHMs and a roll-off of 9.06 dB, despite the difference in their RNs. These results are also summarized in Table 1. It should be noted that the CaF₂-BAP spectrometer produced a broadening of the axial PSF and consequently led to a drop in the sensitivity roll-off, compared with the *benchmark* spectrometer that includes a software interpolation. This result indicates that the imaging performance of spectrometers in OCT applications is sensitive to the effective RN. The benchmark spectrometer originally

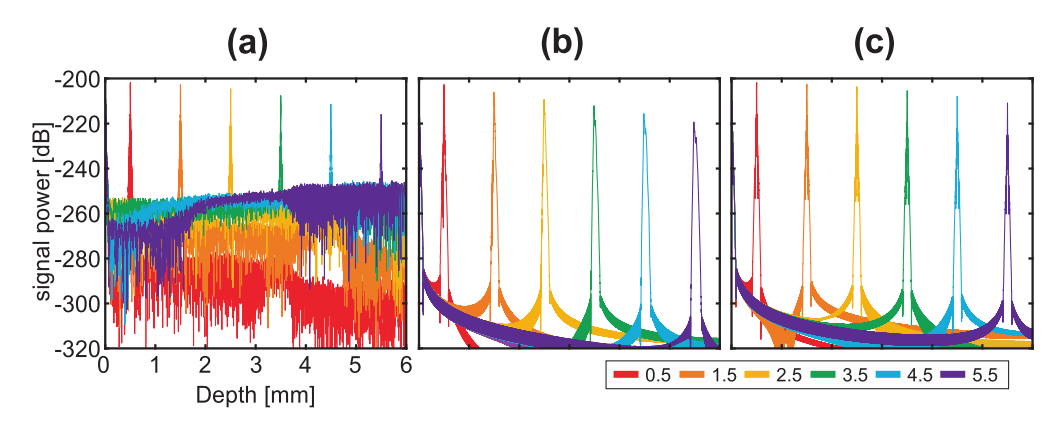


Fig. 6. The axial PSFs with various imaging depths of 0.5, 1.5, 2.5, 3.5, 4.5, and 5.5 mm in the air, for (a) the *benchmark* spectrometer with the linear-*k*-interpolation, (b) CaF₂-BAP spectrometer, and (c) freeform-Design#1 and #2-spectrometers.

had a larger RN than the CaF₂-BAP spectrometer, but this RN was entirely removed with the software interpolation at the cost of interpolation error. Also, this result may appear different from a prior art that shows a roll-off gain by having a prism [4]. There are three major factors contributing to the signal roll-off with imaging depth: 1) The non-linearity in k, 2) the average spectral resolution that is a function of the spot size, the pixel size, and the $d\lambda/dy$, and 3) the variation in spectral resolution across the detector. Unless these factors are explicitly reported, a comparison is specious. Secondly, the reduction in the RN in Design#2 did not further improve the performances of Design#1, which implies that there may be an RN-threshold below which there is no further gain.

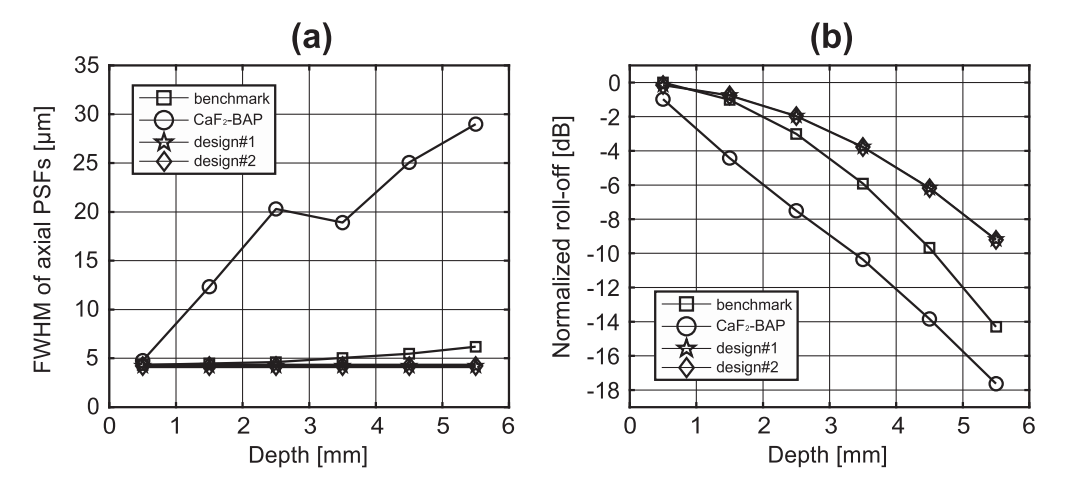


Fig. 7. Imaging performance of the four spectrometer designs: (a) FWHMs of the axial PSFs and (b) normalized peak roll-offs through the imaging depths for the *benchmark* spectrometer with the post-*k*-interpolation and the CaF2-BAP and freeform spectrometers without the post-*k*-interpolation. Note that the performances of Design#1 and #2 are near equivalent, as shown by the overlapping symbols.

To test how the RN was affected by manufacturing tolerances, we performed a Monte Carlo analysis on Design#2. For 10,000 trials, 95% of the outcomes maintained an RN lower than 6×10^{-5} %. This value is similar to the nominal RN of Design#1, so we expect the fabricated Design#2

Table 1. Summary of imaging performance

Spectrometer	Residual nonlinearity [%]	Peak roll-off from 0.5 to 5.5 mm [dB]	FWHMs of the axial PSFs [µm]
benchmark	2.47	14.3	4.3-6.2
CaF ₂ -BAP	0.05	16.7	4.8-29
design#1	2.79×10^{-5}	9.06	4.2
design#2	3.36×10^{-9}	9.06	4.2

to behave similarly to the nominal Design#1. The precision tolerances we applied during the Monte Carlo analysis were (all \pm): 3 fringes of lens-radii error, 0.5 fringes of irregularity, 50 µm of lens-thickness and air-spaces error, 0.0005 refractive-index error, 0.005% Abbe-number error, 10 µm of lens-wedge, 25 µm of lens-decenter, 0.5 mrad of lens-tilt, and 10 µm of double roll. The defocus (\pm 40 µm) and tilt (\pm 7 mrad) of the image plane and axial location of the fiber (\pm 250 µm) were used to recover imaging performance. The decenter of the freeform field lens (\pm 350 µm) was used as a compensator for the k-linearity. We estimate the cost of the freeform element to be around three to five thousand dollars for a single prototype. The cost would significantly be reduced down to a few dollars for production in volume by using a replication or molding technique. Furthermore, the imaging performances of Design#1 and #2 were the same even with the two different RNs. According to our tolerance analysis applied to Design#2, the RN of Design#2 increased to the nominal RN of Design#1. This means that a spectrometer designer should consider choosing a freeform surface design with a lower nominal RN for compensating the influence of manufacturing tolerances.

5. Conclusion

In conclusion, we presented two absolute-linear-in-*k* spectrometer designs with Fringe Zernike freeform field-lenses that showed an invariant 4.2-μm-FWHM axial PSFs as well as a 5.24 dB roll-off gain, i.e., 14.3 dB – 9.06 dB, over the imaging depth from 0.5 to 5.5 mm, compared with the *benchmark* spectrometer of the equivalent spectral resolution. The freeform field-lens corrected both the field-dependent coma and astigmatism caused by the prism in the CaF₂-BAP spectrometer and remarkably reduced the RN to the level where there is no further gain. The RN-threshold for the absolute-*k*-linearity may differ based on the pixel pitch and the spectral dispersion of the spectrometer. The newly demonstrated approach of freeform-optics based optical spectrometers is expected to improve the quality of SD-OCT systems owing to the invariant axial resolution, faster imaging speed, and lower noise.

Funding

University of Rochester; Empire State Development's Division of Science, Technology and Innovation (C160189); Empire State Development (C150130).

Acknowledgments

We thank Andrew Rollins for asking the question of whether freeform optics may be used to linearize spectrometers in k for OCT. We also thank Jonathan Papa, Cristina Canavesi, and Panomsak Meemon for stimulating discussion about this work. We appreciate Synopsys, Inc., for the educational license of CODEV.

Disclosures

The authors declare no conflicts of interest.

References

- S. Vergnole, D. Lévesque, and G. Lamouche, "Experimental validation of an optimized signal processing method to handle non-linearity in swept-source optical coherence tomography," Opt. Express 18(10), 10446–10461 (2010).
- C. Dorrer, N. Belabas, J. P. Likforman, and M. Joffre, "Spectral resolution and sampling issues in Fourier-transform spectral interferometry," J. Opt. Soc. Am. B 17(10), 1795–1802 (2000).
- W. A. Traub, "Constant-dispersion grism spectrometer for channeled spectra," J. Opt. Soc. Am. A 7(9), 1779–1791 (1990).
- Z. Hu and A. M. Rollins, "Fourier domain optical coherence tomography with a linear-in-wavenumber spectrometer," Opt. Lett. 32(24), 3525–3527 (2007).
- V. M. Gelikonov, G. V. Gelikonov, and P. A. Shilagin, "Linear-wavenumber spectrometer for high-speed spectral-domain optical coherence tomography," Opt. Spectrosc. 106(3), 459–465 (2009).
- Y. Watanabe and T. Itagaki, "Real-time display on Fourier domain optical coherence tomography system using a graphics processing unit," J. Biomed. Opt. 14(6), 060506 (2009).
- 7. S. W. Lee, H. S. Kang, J. H. Park, T. G. Lee, E. S. Lee, and J. Y. Lee, "Ultrahigh-resolution spectral domain optical coherence tomography based on a linear-wavenumber spectrometer," J. Opt. Soc. Korea 19(1), 55–62 (2015).
- T. Wu, S. Sun, X. Wang, H. Zhang, C. He, J. Wang, X. Gu, and Y. Liu, "Optimization of linear-wavenumber spectrometer for high-resolution spectral domain optical coherence tomography," Opt. Commun. 405, 171–176 (2017)
- 9. G. Lan and G. Li, "Design of a *k*-space spectrometer for ultra-broad waveband spectral domain optical coherence tomography," Sci. Rep. 7(1), 42353 (2017).
- J. Kalkman, "Fourier-domain optical coherence tomography signal analysis and numerical modeling," Int. J. Opt. 2017, 1–16 (2017).
- A. Bauer and J. P. Rolland, "Design of a freeform electronic viewfinder coupled to aberration fields of freeform optics," Opt. Express 23(22), 28141–28153 (2015).
- A. Bauer, E. M. Schiesser, and J. P. Rolland, "Starting geometry creation and design method for freeform optics," Nat. Commun. 9(1), 1756 (2018).
- J. Reimers, A. Bauer, K. P. Thompson, and J. P. Rolland, "Freeform spectrometer enabling increased compactness," Light: Sci. Appl. 6(7), e17026 (2017).
- K. Fuerschbach, J. P. Rolland, and K. P. Thompson, "Theory of aberration fields for general optical systems with freeform surfaces," Opt. Express 22(22), 26585–26606 (2014).
- 15. K. Emancipator and M. H. Kroll, "A quantitative measure of nonlinearity," Clin. Chem. 39(5), 766-772 (1993).
- K. S. Lee, K. P. Thompson, and J. P. Rolland, "Broadband astigmatism-corrected Czerny–Turner spectrometer," Opt. Express 18(22), 23378–23384 (2010).
- W. Drexler and J. G. Fujimoto, Optical Coherence Tomography-Technology and Applications-2nd Ed. (Springer International Publishing, Switzerland, 2015).